



Numerical Study of Subaortic Stenosis and Pannus Formation on Blood Flow Around Mechanical Heart Valves

Aolin Chen¹, Adi Azriff Basri², Norzian Ismail³, Di Zhu¹, Kamarul Arifin Ahmad^{2,*}

¹ Department of Mechanical, Faculty of Engineering, Universiti Putra Malaysia, Serdang, Malaysia

² Department of Aerospace, Faculty of Engineering, Universiti Putra Malaysia, Serdang, Malaysia

³ Faculty of Medicine and Health Sciences, Universiti Putra Malaysia, Serdang, Malaysia

ARTICLE INFO

Article history:

Received 16 February 2022

Received in revised form 30 April 2022

Accepted 3 May 2022

Available online 3 June 2022

Keywords:

Mechanical heart valve; CFD; heart valve disease; thrombus; pannus

ABSTRACT

Patients after mechanical heart valve implantation are prone to complications. Mechanical heart valve obstruction is a rare but life-threatening complication. Obstruction may include thrombosis, pannus formation around the valve, or both. However, the relationship between thrombus and pannus and mechanical heart valve hemodynamics has not been thoroughly studied. We studied the fluid dynamics of thrombus and pannus formation through numerical simulations and provided detailed information about the interaction between complications and related prosthetic valves so that complications can be detected early. Studies have shown that the formation of thrombus and pannus leads to significant changes in the peak transvalvular velocity of the artificial valve, the transvalvular pressure gradient, and the corresponding hemodynamic indicators. As the height of the thrombus and pannus increases, the jet velocity and transvalvular pressure gradient will increase accordingly. When obstruction exceeds 20%, the impact increases significantly under the same percentage of obstacles. When the obstruction percentage is over 30%, the rest at least doubled. The results also indicate that SAS obstruction has the most significant impact on the blood flow of MHV. At the same time, it should be noted that when SAS and pannus are combined, the ring form vortex in front of the pannus has a potential risk of accelerating the deterioration of the pannus.

1. Introduction

Mechanical heart valve (MHV) is the best choice for patients with heart valve diseases because of its durability [1]. However, obstruction after the MHV replacement surgery is not uncommon. A single jet generated by the unnatural flow of MHV forms three highly turbulent jets through the valve. The reflux volume of MHV is higher than that of a bioprosthetic valve. The non-physiological flow pattern around MHV is caused by its mechanical leaflet geometry, implantation direction and angle. Those are important causes of artificial heart valve dysfunction, higher wall shear stress formed on

* Corresponding author.

E-mail address: aekamarul@upm.edu.my

<https://doi.org/10.37934/arfmts.95.2.180190>

the aortic [19], which can cause severe hemodynamic damage and some complications from the growth of abnormal tissues around the MHV.

Sub-valvular aortic stenosis (SAS), also known as subaortic stenosis (SAS). Described as the membrane (usually the sarcolemma) in front of the aortic valve at some distance that can obstruct blood flow through the left ventricular outflow tract [2]. Therefore, the outflow gradient through the valve becomes higher. According to the shape of obstacles, SAS is divided into three types. The first type is thin crescent-shaped membrane. The second type is thick fibrous muscle ridges. The third type is a tunnel or tube [9]. The presence of SAS may add extra load to the left ventricle, thereby increasing the risk of sudden death from ventricular fibrillation. The recurrence rate of SAS after surgery is as high as 37% [10]. Previous numerical studies focus on the regular and dysfunctional MHV with the velocity field, vortex dynamics, turbulence characteristics, leaflet dynamics, and its relationship with platelet activation and/or hemolysis. Numerical results show that pressure changes are also significantly affected by stenosis [18], and WSS is relatively high in stenosis [16].

Pannus formation is an important cause of leaflet dysfunction after artificial heart valve replacement [3]. Pannus is an abnormal layer of fibrovascular tissue or granulation tissue, usually located in the ring position, growing from the sewing ring to the center of the MHV on the left ventricle side. Pannus formation will disrupt the transvalvular blood flow and cause valve dysfunction or stenosis, which is considered the source of high transvalvular pressure drop. These high-pressure drops and reflux are dangerous because they can cause irreversible damage to the left ventricular muscles [8]. Valve insufficiency and intermittent valvular regurgitation can occur in patients with the valvular disease even when there is no physical valve-to-valve contact [11]. This indicates that the flow disturbance caused by the pannus should be the main reason for the incomplete movement of the blade. Some studies suggest better engraftment of MHVs based on hemodynamic characteristics, such as MHV pressure drop, regurgitation, and damage to red blood cells and plates.

Symptoms vary depending on the severity of the valve blockage. SAS can lead to severe heart failure or embolism. In hyperproliferation of the pannus, the MHV leaflets may become obstructed. Leaflet dysfunction is a rare but life-threatening complication [4]. However, SAS must be distinguished from pannus. These two mechanisms are often misdiagnosed and confused. They have a typical outcome leading to obstruction of the mitral valve prosthesis [5]. Mechanical prosthesis partial thrombosis, overgrowth of peripheral pannus, and transesophageal echocardiography showed mechanical prosthesis occlusion.

Although echocardiography is the method of choice for evaluating prosthetic valve occlusion, its usefulness is limited by metal artifacts in MHV and is not suitable for detecting the exact cause of valve occlusion, such as SAS, pannus, or others [6]. Numerical simulation of blood has become an effective method to study blood flow in mechanical heart valves. Suspected prosthetic valve obstruction requires rapid diagnostic evaluation. The treatment strategy will be affected by the position of the prosthesis, the severity of the valve obstruction, and the patient's clinical condition. In cases of mechanical valve obstruction, repeated surgery is the first-line treatment. In non-obstructive cases, thrombolysis or fibrinolysis is a viable alternative, but the other complications must be considered [7].

In this study, we aimed to investigate the influence of MHV obstruction formation on the mechanical function of MHV and its hemodynamic characteristics, then compare the flow characteristics caused by the formation of subaortic stenosis, pannus, and both combinations. Although the simulations simplify the geometry of the aorta and cannot fully reproduce in vivo conditions, they can provide a preliminary study of the effect of MHV occlusion formation on hemodynamic properties. Finally, the relationship between the obstruction of the MHV and the

percentage of SAS and pannus was investigated, and the minimum vascular obstruction range required to induce severe aortic valve stenosis in patients with the MHV was determined.

2. Methodology

The construction of the MHV model will be demonstrated in this part. In addition, the numerical method, boundary conditions, and governing equations are also discussed.

2.1 Geometry

This study used the 23mm On-X heart valve, which is one of the most promising MHV. The model was created with SolidWorks software, and the structural data was generated from Mirkhani N *et al.*, [12]. Show as in Figure 1 the simulation includes four main parts: front aortic, MHV, Valsalva sinus, and back aortic.

Three case models are built to compare with the healthy mechanical heart valve, case1 is SAS, case 2 is pannus, and case 3 is combined with both SAS and pannus. Each case has four groups with different obstruction percentages, 10%, 20%, 30%, and 40%, depending on the high obstruction.

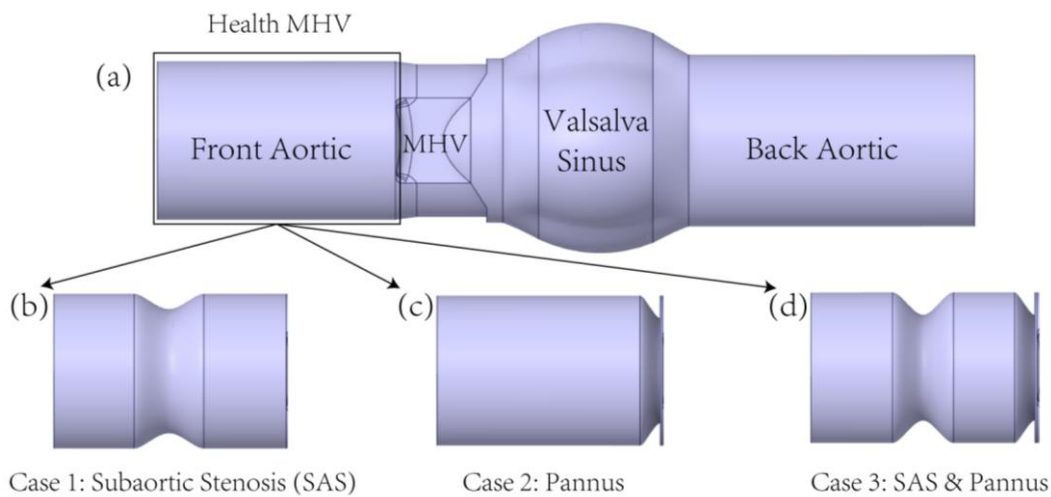


Fig. 1. MHV structure and Obstruction (case1: SAS, case2: pannus, case3: both combine)

2.2 Boundary Conditions

The fluid boundary conditions were derived from previous numerical simulations of the flow through the MHV in an aortic physical environment [13]. The simulation was performed under pulsatile conditions with an experimental pulsatile flow as an inlet condition. It enforced typical physical flow conditions of about 25 L/min peak flow rate, 0.86s cardiac cycle, one-third of which is the systolic length shown in Figure 2. There are two important phases, T1 (0.1s) is the mid-accelerated phase, and T2 (0.2s) is the peak phase. In addition, the outlet condition was at the ambient pressure for all cases, and a no-slip condition at the walls was adopted.

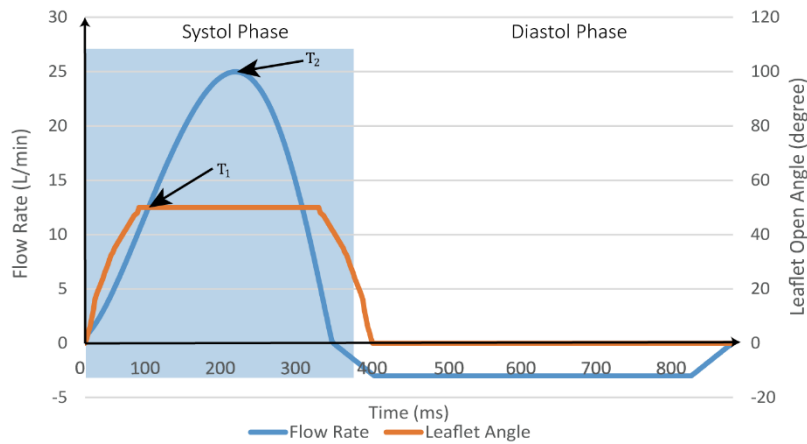


Fig. 2. Flow rate pulse of the aorta inlet and Leaflet open angel changes. Points T1 and T2 indicate critical instances of time at which the flow characteristics

2.3 Governing Equation

OpenFOAM open-source toolbox with the pimpleFoam unsteady incompressible solver is used in this study. The pimpleFoam is the combination of PISO (Pressure Implicit with Splitting of Operator) and SIMPLE (Semi-Implicit Method for Pressure-Linked Equations) algorithms [14]. The blood is assumed to be incompressible fluid with the equation of continuity and momentum as follows

$$\nabla \cdot u = 0 \tag{1}$$

$$\frac{\partial(\rho u)}{\partial t} + \nabla \cdot (\rho u u) - \nabla \cdot (\mu \nabla u) - (\nabla u) \cdot \nabla \mu = -\nabla p \tag{2}$$

where u is velocity vector, p is pressure, μ is viscosity, and ρ is density. The density value is considered as 1060 kg/m^3 . The NS equations are combined with an appropriate non-Newtonian constitutive model of dynamic viscosity to simulate blood shear thinning behavior. Well known Carreau model was used [15]. The equation shows as follows

$$\eta(\dot{\gamma}) = \eta_{\infty} + (\eta_0 - \eta_{\infty}) [1 + (\lambda \dot{\gamma})^a]^{\frac{n-1}{a}} \tag{3}$$

where: $\eta_0 = 0.56 \text{ Pas}$ $\eta_{\infty} = 0.0035 \text{ Pas}$ $\lambda = 8.2$ $n = 0.2128$ $a = 2$

Compared with the Newtonian model, the verification in terms of shear rate, streamlines, vorticity, and other parameters, the non-Newtonian model is necessary [17].

2.4 Simulation method

In this study cfMesh tools used to generate mesh, cfMesh is a library for mesh generation implemented within the OpenFOAM framework. In meshDict can be divided into mandatory settings (surfaceFile and maxCellsize) and local refinement (boundaryCellsize and localRefinement), and the mesh results are shown in Figure 3. The grid independence is verified by five groups of different grid numbers, compared by the maximum WSS obtained on the wall as shown in Figure 4. When the number of grids reaches about three million, the WSS reaches stability. No significant change in WSS

as the number of grids continues to increase. Each case requires about 18h per simulation on a workstation with two Intel Platinum 8171M 3Ghz-processors and 128GB of RAM.

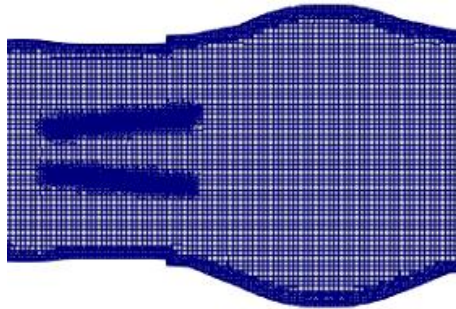


Fig. 3. Mesh quality of MHV model

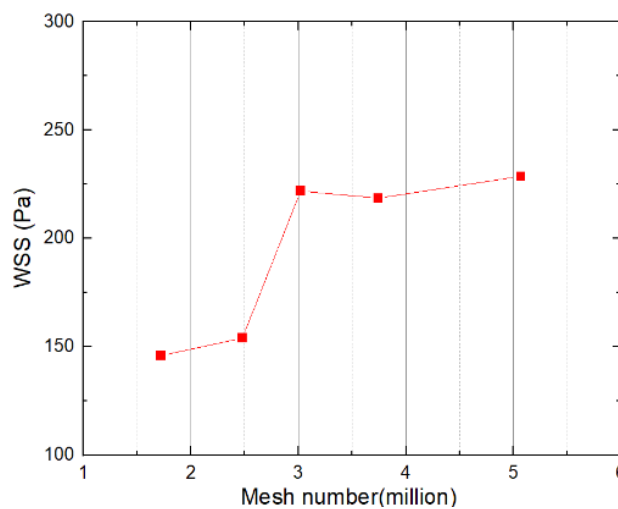


Fig. 4. Mesh independence verification (WSS)

3. Results

3.1 Velocity Contours

Figure 5 below shows the MHV center-cut view velocity contour in three cases compared with HMHV at two different time instants (T1 at 0.1s (acceleration phase) and T2 at 0.2s (peak phase)) during the systole phase, for SAS, pannus, and combustion at different percentage obstruction (10%, 20%, 30%, and 40%). The velocity field at the mechanical heart valve changes significantly depending on pannus and subaortic stenosis severity. Under normal MHV, the flow field at the exit of the MHV has three independent jets from both sides and a central hole. SAS, pannus, and both combustions will lead to the velocity change. The peak velocity magnitude was proportional to the severity. Peak velocity change with the dysfunction percentage is shown in Figure 6. The maximum velocity of Severe subaortic stenosis was increased from 1.87m/s to 3.96m/s (+112%) at 40% obstruction, and in the case of pannus was increased from 1.87 to 4.81(+157%) at 40% obstruction, in the combined of subaortic stenosis and pannus case was increased from 1.87 to 4.57(+144%). As the percentage of blockage increases, the pannus has the greatest impact on velocity, resulting in the most significant acceleration.

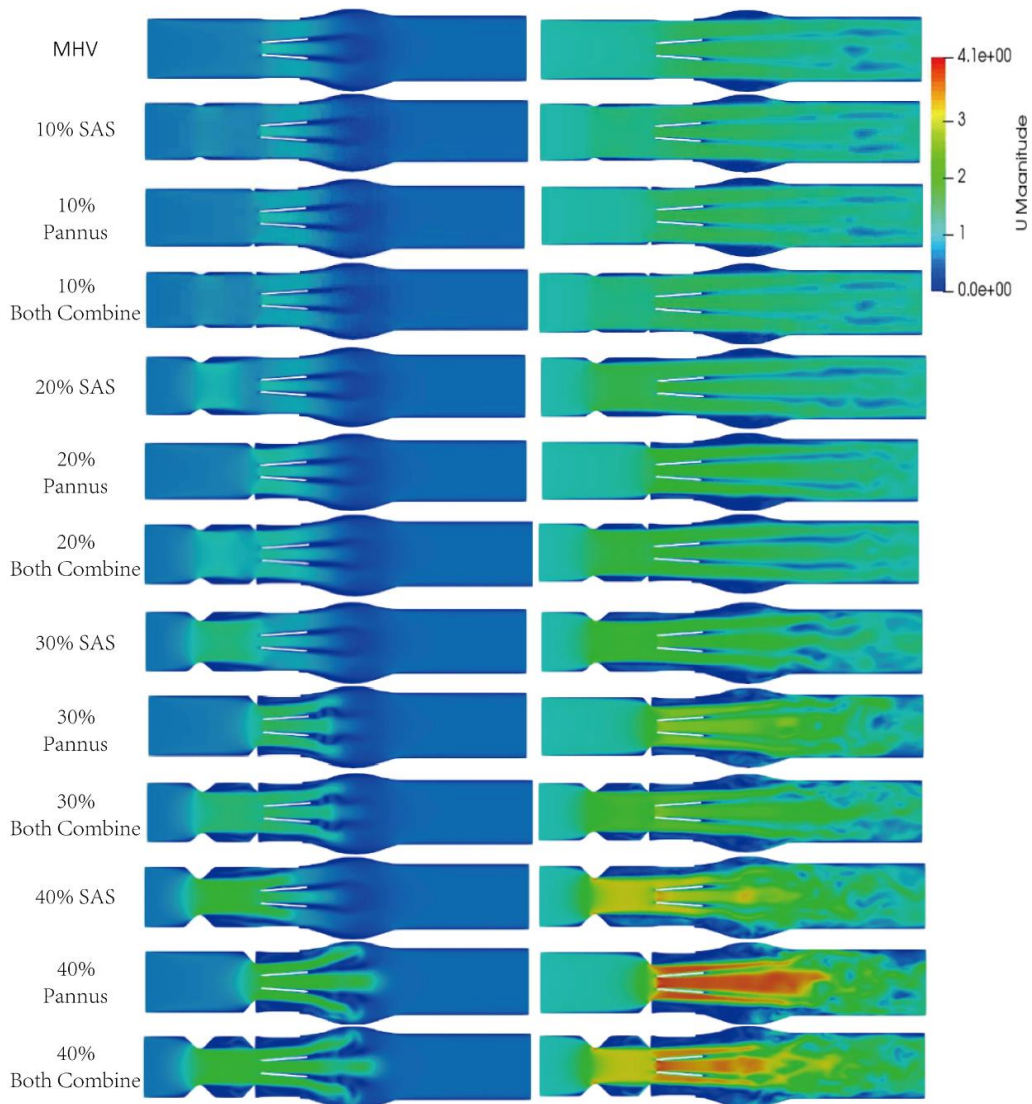


Fig. 5. Velocity contour at SAS, pannus and both combination in different percentage blockage (10%, 20% 30% and 40%) at T1 and T2

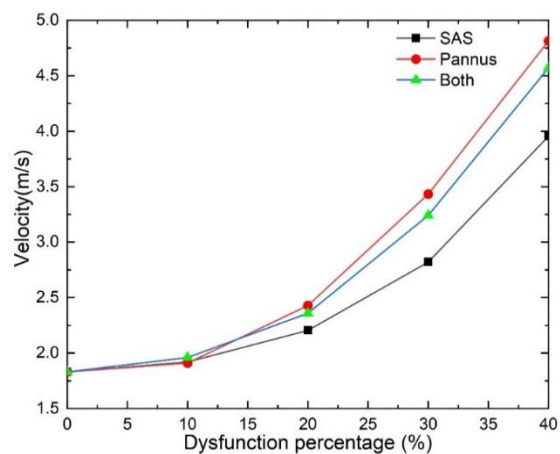


Fig. 6. Maximum velocity vs blockage percentage at T2

Figure 7 shows the velocity distribution over the centerline. The velocity shows a significant acceleration when blood flows through the pannus and SAS obstruction. After the SAS accelerates, the blood flow velocity decreases, and a secondary acceleration occurs when passing through the MHV entrance. In the case of pannus, due to the overlap of pannus and MHV entrances, only one significant acceleration occurs here in the case of subaortic stenosis and pannus both combined, the velocity contour similarly to case1, blood flow velocity slightly decreases after passing through the subaortic stenosis, and a second acceleration occurs when passing through the pannus. However, the overall acceleration is lower than the speed increase in the case of the pannus alone.

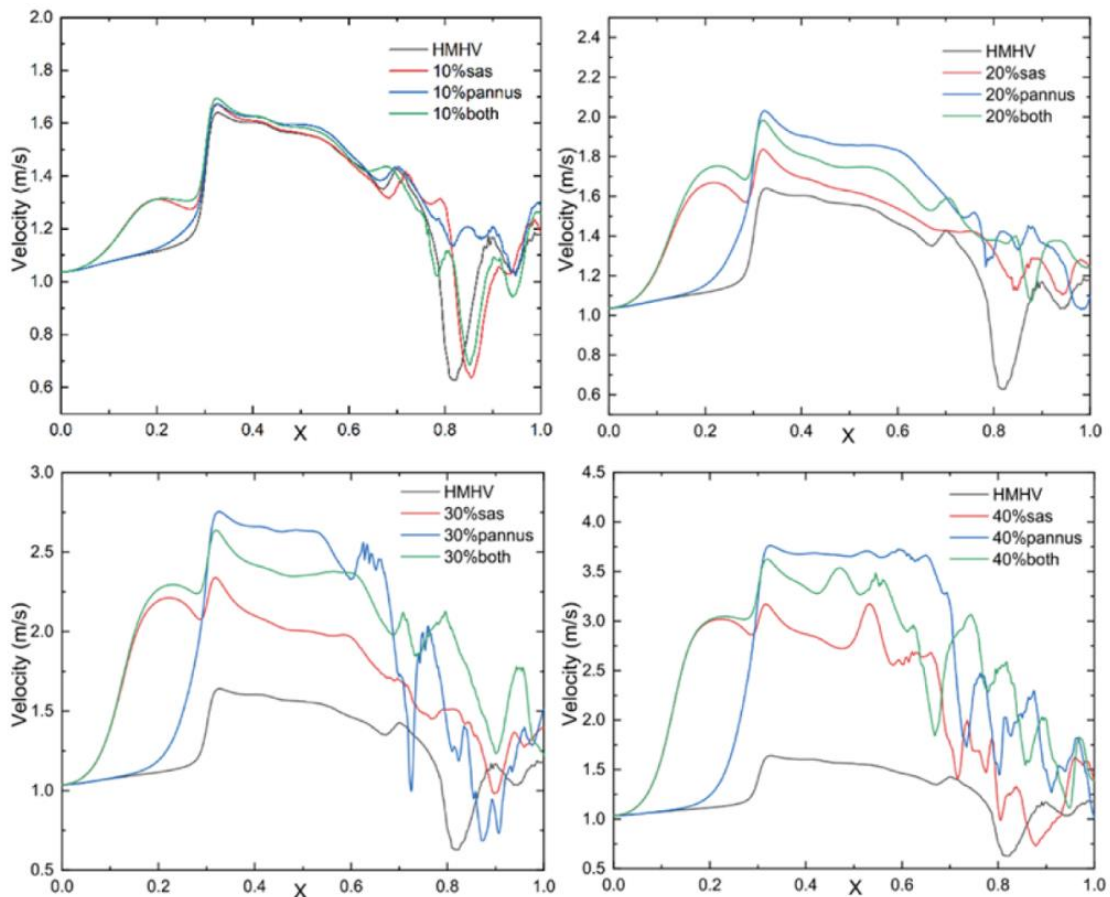


Fig. 7. Velocity over the center line of MHV at T2

3.2 Vortex Dynamic

Figure 8 shows the vortex formation for SAS, pannus, and both combustion cases at T2. Vortex structure was dependent on the severity of subaortic stenosis and pannus. A dominant vortex is formed in the Valsalva sinus area behind the valve. The vortex shedding mechanism (V-shaped on the Karman vortex street) is observed in all models, and its intensity is proportional to the severity of subaortic stenosis and pannus. In subaortic stenosis cases, the vortex structure forms complex vortices in the Valsalva sinus. In the pannus case, the complex vortices move backward, mainly around the back sinus region. However, when SAS and pannus are combined, vortices are not only formed downstream of pannus. Moreover, a vortex structure is also formed upstream of the pannus. The intensity, coverage area, and vortex structures have significantly increased regardless of the condition.

The magnitude of the vorticity is proportional to the degree of LVOT blockage and the eddy current shedding mechanism at the trailing edge of the BMHV. The location of the sinus area and the recirculation area downstream of the valve is related to the obstruction.

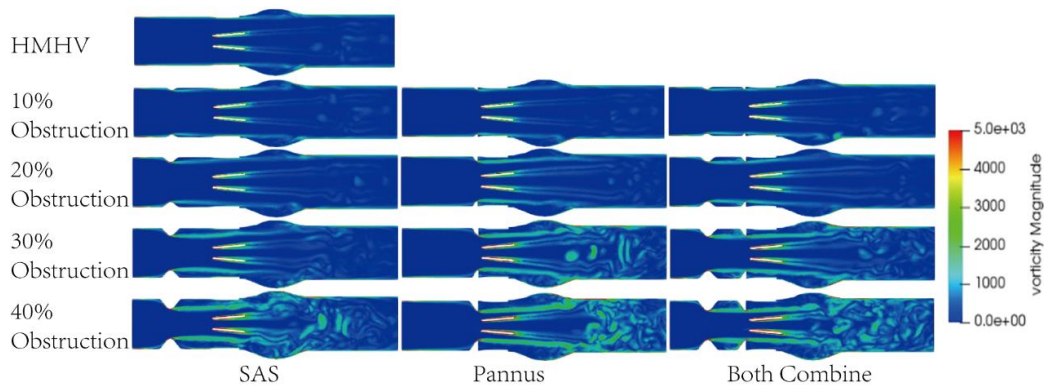


Fig. 8. Vorticity distributions downstream at peak time (T2)

3.3 Pressure Drop

Figure 9 shows the pressure along the centerline of the flow direction without obstruction. The pressure before the anterior edge of the valve leaflet drops rapidly. That's due to the installation of the MHV, passing through the MHV and the Valsalva sinus almost constant, and ascending in the aorta. The pressure is nearly constant, passed through the MHV and sinus of Valsalva, and recovers in the ascending aorta. The presence of SAS and pannus significantly increases the pressure drop and increases with the increase in the percentage of obstruction. Among the three types of obstruction, the pressure drop of the pannus is the largest, and the obstruction surface of the pannus overlaps with the aortic ring, resulting in only a large-area annular obstruction in the entire fluid channel. The increase in occlusion percentage resulted in a parabolic increase in TPG, mainly due to increased maximum velocity at the prosthetic valve exit. At 40% obstruction in Figure 10, the TGP of pannus was approximately 8-fold higher than that of non-obstructed TGP, and the TGP of SAS was approximately 6-fold higher. The increase is also obvious, but the TGP caused by pannus is higher under the same obstruction percentage.

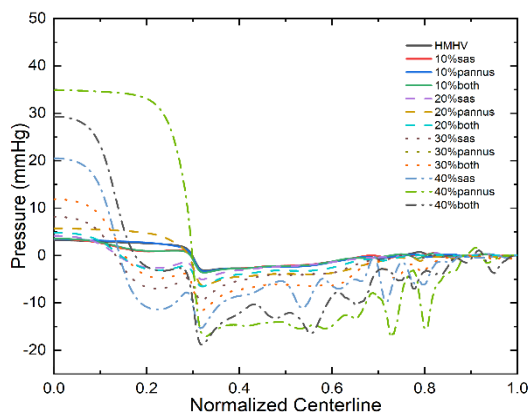


Fig. 9. Pressure drops in the direction of blood flow

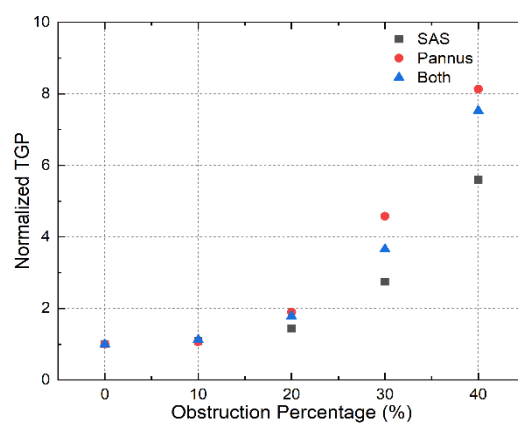


Fig. 10. NTGP VS obstruction

3.4 Wass Shear Stress

When there is no obstruction in MHV, there is a lower maximum wall shear stress (WSS) (approximately 225Pa) on the walls and leaflets during the peak phase. As the obstruction percentage increases, the maximum WSS value shows a parabolic increase. As shown in Figure 11, the largest increase in WSS is caused by the Pannus obstruction. When the obstruction percentage increases to 40%, the maximum WSS is 3.14 times that without obstruction. The maximum WSS increases the slowest under the SAS barrier and is about 2.5 times. The average WSS has a similar trend. However, at 10% obstacles, the average WSS will be slightly lower than the average WSS when there are no obstacles. That is due to the obstruction blockage of the blood flow; the velocity decreased and showed laminar flow when passing through the 10% obstruction, lower velocity and without vortex formed at the obstruction back region lead to lower WSS. Eventually, the average WSS at 10% obstruction is lower than the MHV without obstruction. When the obstruction exceeded 20%, pannus caused the largest increase in WSS and the smallest change in SAS for the same percentage of obstruction, and when the two were combined, the change was in the middle.

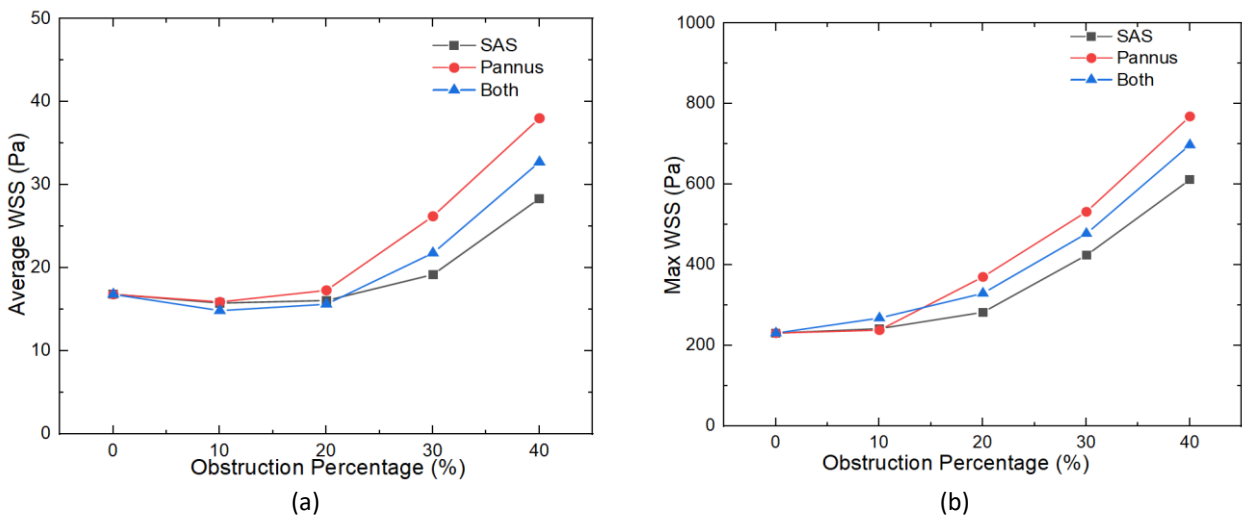


Fig. 11. WSS VS obstruction percentage (a) Average WSS (b)Max WSS

4. Conclusions

This study investigates the effect of MHV obstruction (SAS, pannus, and combined) on MHV mechanical function and its hemodynamic properties. The results showed that obstruction in the three cases would significantly impact hemodynamics, manifested by increased flow velocity, pressure drop, WSS, and vorticity. Especially when SAS and pannus are combined, they form an apparent vortex structure before pannus, increasing the risks of platelet activation and/or hemolysis. When obstruction exceeds 20%, the impact increases significantly under the same percentage of obstacles. Starting from 30% obstruction, all values at least doubled. Pannus has the greatest impact, with a maximum velocity increase of 157% at 40% obstruction, a maximum WSS increase of 3.14 times, SAS has the least impact, a maximum velocity increase of 112%, and a maximum WSS increase of 2.5 times. When the two coexist, the impact is in the middle of the two, the maximum velocity increases by 144%, and the maximum WSS increases by 2.85 times. The results also indicate that SAS obstruction has the greatest impact on the blood flow of MHV. At the same time, it should be noted that when SAS and pannus are both combined, the vortex in front of the pannus has a potential risk of accelerating the deterioration of the pannus.

Acknowledgment

This research was not funded by any grant. The authors would like to express their gratitude and sincere gratitude to the Department of Aerospace Engineering, Faculty of Engineering, Universiti Putra Malaysia for their close cooperation in this work. I would also like to thank the supervisor and co-supervisor for their help.

Reference

- [1] Choudhary, Shiv Kumar, Sachin Talwar, and Balram Airan. "Choice of prosthetic heart valve in a developing country." *Heart Asia* 8, no. 1 (2016): 65-72. <https://doi.org/10.1136/heartasia-2015-010650>
- [2] Kelly, D. T., E. Wulfsberg, and RICHARD D. ROWE. "Discrete subaortic stenosis." *Circulation* 46, no. 2 (1972): 309-322. <https://doi.org/10.1161/01.CIR.46.2.309>
- [3] Moldovan, Maria-Sînziana, Daniela Bedeleanu, Emese Kovacs, Lorena Ciomărnean, and Adrian Molnar. "Pannus-related prosthetic valve dysfunction. Case report." *Clujul Medical* 89, no. 1 (2016): 169. <https://doi.org/10.15386/cjmed-510>
- [4] Khan, Nasir A., Jagdish Butany, Shaun W. Leong, Vivek Rao, Robert J. Cusimano, and Heather J. Ross. "Mitral valve-sparing procedures and prosthetic heart valve failure: a case report." *Canadian Journal of Cardiology* 25, no. 3 (2009): e86-e88. [https://doi.org/10.1016/S0828-282X\(09\)70050-9](https://doi.org/10.1016/S0828-282X(09)70050-9)
- [5] Roudaut, Raymond, Karim Serri, and Stephane Lafitte. "Thrombosis of prosthetic heart valves: diagnosis and therapeutic considerations." *Heart* 93, no. 1 (2007): 137-142. <https://doi.org/10.1136/hrt.2005.071183>
- [6] Ivaniv, Yuriy. "Echocardiographic evaluation of heart valve prosthetic dysfunction." *Heart, Vessels and Transplantation* 2, no. 1 (2018): 10-16. <https://doi.org/10.24969/hvt.2017.46>
- [7] Bonou, Maria, Konstantinos Lampropoulos, and John Barbetseas. "European Heart Journal: Acute Cardiovascular." *European Heart Journal: Acute Cardiovascular Care* 1, no. 2 (2012): 122-127. <https://doi.org/10.1177/2048872612451169>
- [8] Kim, Woojin, Haecheon Choi, Jihoon Kweon, Dong Hyun Yang, and Young-Hak Kim. "Effects of pannus formation on the flow around a bileaflet mechanical heart valve." *Plos one* 15, no. 6 (2020): e0234341. <https://doi.org/10.1371/journal.pone.0234341>
- [9] Devabhaktuni, Subodh R., Eyas Chakfeh, Ali O. Malik, Joshua A. Pengson, Jibrán Rana, and Chowdhury H. Ahsan. "Subvalvular aortic stenosis: a review of current literature." *Clinical cardiology* 41, no. 1 (2018): 131-136. <https://doi.org/10.1002/clc.22775>
- [10] Jonas, Richard A. "Modified Konno procedure for tunnel subaortic stenosis." *Operative Techniques in Thoracic and Cardiovascular Surgery* 7, no. 4 (2002): 176-180. <https://doi.org/10.1053/otct.2003.36320>
- [11] Lindman, Brian R., Marie-Annick Clavel, Patrick Mathieu, Bernard Lung, Patrizio Lancellotti, Catherine M. Otto, and Philippe Pibarot. "Calcific aortic stenosis." *Nature reviews Disease primers* 2, no. 1 (2016): 1-28. <https://doi.org/10.1038/nrdp.2016.6>
- [12] Mirkhani, Nima, Mohammad Reza Davoudi, Pedram Hanafizadeh, Daryoosh Javidi, and Niloofar Saffarian. "On-X heart valve prosthesis: numerical simulation of hemodynamic performance in accelerating systole." *Cardiovascular engineering and technology* 7, no. 3 (2016): 223-237. <https://doi.org/10.1007/s13239-016-0265-y>
- [13] Borazjani, Iman, Liang Ge, and Fotis Sotiropoulos. "Curvilinear immersed boundary method for simulating fluid structure interaction with complex 3D rigid bodies." *Journal of Computational physics* 227, no. 16 (2008): 7587-7620. <https://doi.org/10.1016/j.jcp.2008.04.028>
- [14] Onel, Huseyin C., and Ismail H. Tuncer. "A comparative study of wake interactions between wind-aligned and yawed wind turbines using LES and actuator line models." In *Journal of Physics: Conference Series*, vol. 1618, no. 6, p. 062009. IOP Publishing, 2020. <https://doi.org/10.1088/1742-6596/1618/6/062009>
- [15] Kim, Sun Kyoung. "Collective viscosity model for shear thinning polymeric materials." *Rheologica Acta* 59, no. 1 (2020): 63-72. <https://doi.org/10.1007/s00397-019-01180-w>
- [16] Miah, Md Abdul Karim, Shorab Hossain, and Sayedus Salehin. "Effects of Severity and Dominance of Viscous Force on Stenosis and Aneurysm During Pulsatile Blood Flow Using Computational Modelling." (2021). <https://doi.org/10.37934/cfdl.12.8.3554>
- [17] Al-Azawy, Mohammed Ghalib, Saleem Khalefa Kadhim, and Azzam Sabah Hameed. "Newtonian and non-newtonian blood rheology inside a model of stenosis." *CFD Letters* 12, no. 11 (2020): 27-36. <https://doi.org/10.37934/cfdl.12.11.2736>
- [18] Basri, Adi Azriff, SM Abdul Khader, Cherian Johny, Raghuvir Pai, Mohammed Zuber, Zainuldin Ahmad, and Kamarul Arifin Ahmad. "Effect of single and double stenosed on renal arteries of abdominal aorta: A computational fluid dynamics." *CFD Letters* 12, no. 1 (2020): 87-97.

- [19] Salleh, Nursyaira Mohd, Mohamad Shukri Zakaria, Mohd Juzaila Abd Latif, and Adi Azriff Basri. "A Computational Study of a Passive Flow Device in a Mechanical Heart Valve for the Anatomic Aorta and the Axisymmetric Aorta." *CFD Letters* 13, no. 4 (2021): 69-79. <https://doi.org/10.37934/cfdl.13.4.6979>